2022 IEEE International Autumn Meeting on Power, Electronics and Computing (ROPEC) | 978-1-6654-5892-4/22/$31.00 ©2022 IEEE | DOI: 10.1109/ROPEC55836.2022.10018744

Theoretical and experimental investigation of a Faraday disc generator

Jorge Luis Galvan-Ruiz
F. Sergio Sellschopp-Sanchez
Carlos Álvarez-Macías
TecNM / Instituto Tecnológico de La Laguna
Torreón, México
jorgegalvan@live.com.mx, fsellschopps@correo.itlalaguna.edu.mx

Rodrigo Loera
CONACYT - TecNM / Instituto Tecnológico de La Laguna
Torreón, Mexico

Raúl A. Ávalos-Zúñiga
Centro de Investigación en Ciencia Aplicada y Tecnología Avanzada
Unidad Querétaro - IPN
Querétaro, Mexico

Michel Rivero
Instituto de Investigaciones en Materiales
Unidad Morelia - UNAM
Morelia, Mexico
mrivero@materiales.unam.mx

***Abstract*—This work deals with the case of a ring-shaped conductive solid material rotating at different speeds in a constant magnetic field. Their interaction induces a potential difference between the inner and outer radius of the disc, which is measured. This configuration corresponds to a Faraday's disc. It is important to understand the phenomena of electromagnetic induction for small-scale direct current generators, as Faraday's disc. These kinds of generators allow replacing the use of batteries employed on micro-scale applications such as small signal monitoring, medical apparatus inserted in human bodies, smart textile and smart skin devices that can monitor mechanical and thermal variables in the human body, etc. For these applications, it is of great importance to fully understand the underlying physics of these generators, for which experimental and theoretical analysis is employed. The generator's conceptual application in future stages is to collect the untapped kinetic energy found in several physical systems such as human body movement, and vibrations on machinery, among others.**

In this work, a Faraday's disk generator is analyzed experimentally and theoretically to understand the fundamental aspects of these devices. This allows for validating the theoretical models, which can be used to determine the output electrical variables (electric power, induced voltage, and current) of the system operating under given experimental conditions. Comparison results among experimental and analytical models are shown.

Keywords- Generator, energy harvesting, modeling.

I. Introduction

In recent years, wind and photovoltaic solar energy have shown the greatest growth among the various forms of energy. Energy is available from the environment in a wide variety of forms, such as chemical, thermal, and radioactive, among others. This work is about untapped energy. The conversion of waste energy into other useful forms, or energy harvesting, represented about 1.3% of the energy generated in 2021, as shown in Figure 1. The environment is a system built up of more subsystems interacting with each other, in which energy is continuously transformed from one type to another. In this context, there exist several forms in which kinetic energy is available in the environment. Forms are as diverse as the different natural resources.

The human body, as well as a large number of industrial processes and everyday technological applications, are an unlimited source of small amounts of "unused" (sometimes also referred to as *wasted*) energy [2]. This energy is currently harnessed

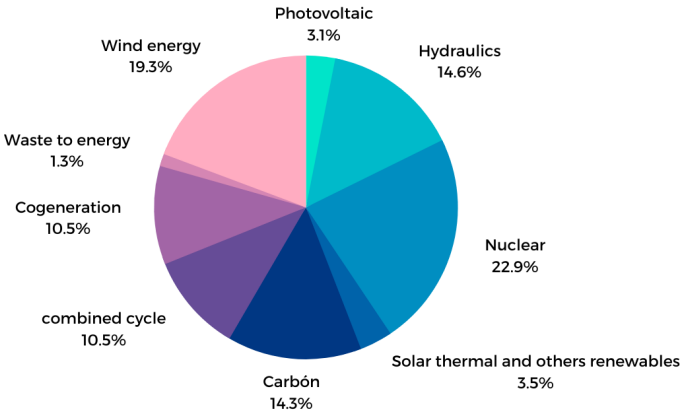

Fig. 1. Kind of energy generated in 2021 (data taken from [1])

through different means such as nano-generators [3]. Generators are mainly based on *piezoelectricity* [4], in which deformations produced by some forcing element, such as footsteps, are used to produce electricity, *triboelectricity* [5], based on the friction of one material to another to produce energy, or *electromagnetic effects* [6].

The rapid growth of miniaturized electronics, networked smart electronic devices, and the internet of things, require reliable power sources such as batteries. Nevertheless, the use of batteries poses several technological and environmental concerns. For example, a billion IoT devices that work with batteries imply 274 million battery changes per day [7], [8]. Among the different kinetic energy sources, a particular interest exists in the kinetic energy produced by the movement of the human body. Energy harvesting from human motion represents a promising alternative to power supply for portable and wearable electronic devices and prosthetics [9].

Several configurations have been proposed for energy harvesting of human motion, among which is the vortex-type MHD

generator [10], which can withstand high pressure and aperiodic movement. In this case, the fluid is confined between two electrically conducting concentric cylinders and moves in the azimuthal direction, while the whole system is immersed in an axial magnetic field. This system leads to complex three-dimensional flows [10]. This 3D flow can be simplified by considering the fluid as an ideal electrically conductor performing a rigid rotation. In this case, the system reduces to the Faraday disc generator [11]. This generator can be constructed and characterized in a laboratory and a systematic investigation helps in understanding the underlying phenomena. These are valuable not only as a starting point toward designing electric power devices but also as a teaching resource.

In this work, a systematic analysis of a Faraday disc generator is carried out. This system consists of a rotating disc (made of aluminum) in the presence of a magnetic field produced by a disc-shaped permanent magnet that is at rest. The interaction of the rotating disc and the magnetic field induces electric currents in the radial direction, which can be measured. This work is divided as follows. Section II describes the experimental setup and conditions of the Faraday disc generator. The theoretical model is resumed in Section III. Then, the theoretical and experimental results are compared and discussed in Section IV. In this section, the effect on the induced voltage, current and electric power of the disc's rotation speed under open circuit conditions are addressed, while the effect of the external load is investigated theoretically. The final comments are provided in Section V.

II. Experimental Setup

The experimental setup consists of a rotating aluminum disc immersed in a magnetic field, as shown in Figure 2. The disc, located in front of the magnet, is driven by a 12 V dc motor. The disc is attached to a nylamid piece, which electrically isolates it from the aluminum shaft (1.9 cm diameter and 35 cm long). The magnetic field is produced by a disc-shaped permanent magnet magnetized in the axial direction, rigidly fixed to a nylamid static support, and placed at a specific distance from the disk. The shaft, magnet, and disc are aligned along the axis and the whole system is mounted on a plywood base. The CAD model and the picture of the experiment are presented in Figures 2(a) and 2(b), respectively.

The dc motor allows obtaining rotation speeds ranging from 1200 to 2400 RPM. The dimensions of the disc and magnet are shown in figure 2. Their properties and geometrical parameters are presented in Table I.

TABLE I
Main Physical and Geometrical Parameters

Characteristic	Value
Inner radius	2.5 mm
Outer radius	25 mm
Height	2 mm
Disc material	Aluminum
Electrical conductivity	37.8×10^6 S m^{-1}
Disc magnet ($r \times H$)	25.4×10 mm
Magnetic flux density	131 mT

A. Experimental characterization

The experimental stage consists of applying different speeds to the motor that moves the Faraday disk in order to measure the induced potential in the internal and external radii of the disk. To instrument the experiment, an optical speed sensor mounted on the shaft that moves the disc and a tension meter based on a portable digital oscilloscope and the electrodes that collect the tension between these two radii of the Faraday disc were used. The setup addressed in this work focuses only on the open-circuit condition, while other load conditions are explored theoretically.

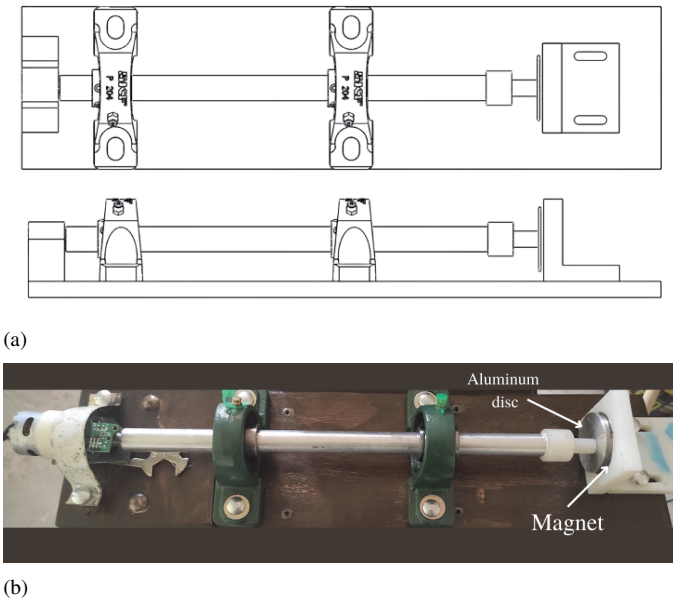

(a)

(b)

Fig. 2. (a) Scheme of the top and side view of the system, and (b) physical model

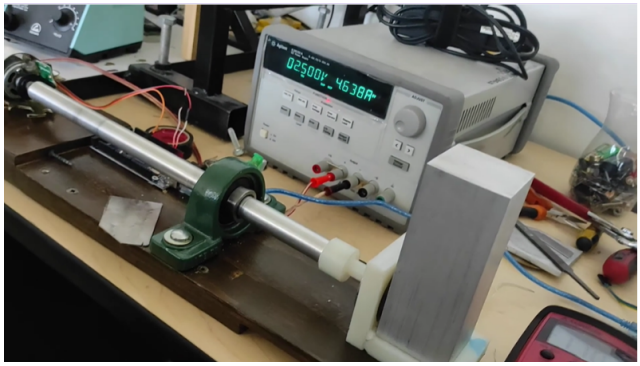

Fig. 3. View of the development of the experiment.

1) Rotational speed measure: A 20-segment digital optic sensor LM6490 coupled to the aluminum shaft was used to register the speed rotation, and an Arduino board was used to read and record the sensor data, each measure reports the mean value of 1.5 minutes measurement with a sampling rate of one second. Figure 3 shows a complete image of the running experiment. A voltage source CC Agilent/Keysight E3632A is used to power the dc motor and drive the disc at the desired rotation speed.

2) Induced voltage: The induced voltage was measured under open-circuit conditions. Measurements were done using two electrodes located at the external radius and as close as possible to the inner radius, as shown in figure 5. The voltage was recorded using a handheld oscilloscope Rohde&Schwarz RTH1004 and the data were post-processed to obtain the averages of the values.

III. Theoretical Model

The analytical modeling addressed in the paper is based on the ideal flow, detailed on [10], which coincides with the case of a rotating solid body. The system considers a ring-shaped solid of

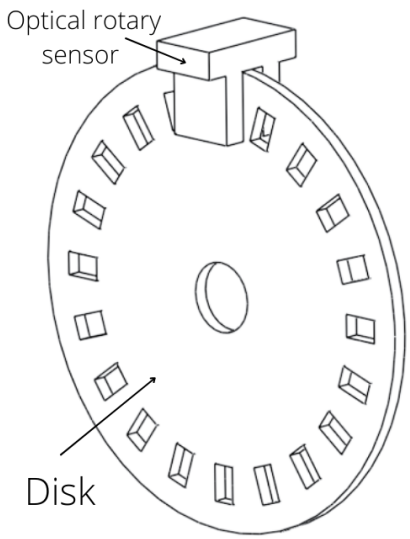

Fig. 4. Scheme of the optical rotary sensor

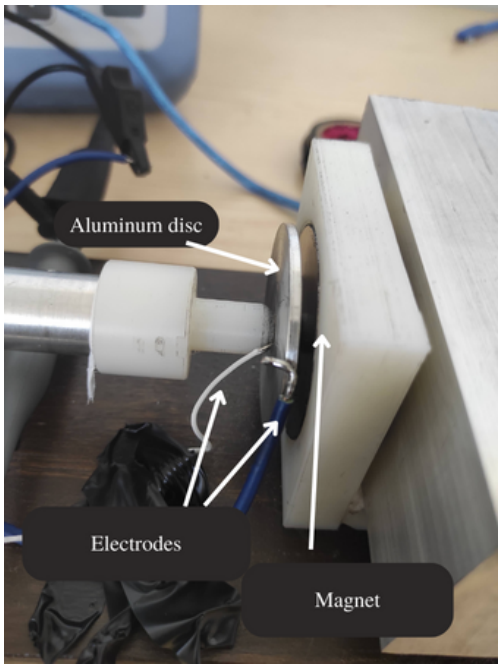

Fig. 5. Picture showing the position of the electrodes during measurements.

internal and external radius r_i and r_o, and height H, as shown in figure 6. The solid is immersed in a constant axial magnetic field and rotates at a constant speed ω. Therefore, the azimuthal velocity is $u_\theta(r) = \omega r$. The interaction of the rotating ring and the applied magnetic field induces an electric potential drop in the radial direction, which can be measured.

A generator with the configuration presented in figure 6 corresponds to the classic Faraday disc generator. If the solid rotates with a velocity u_θ, it follows that the volumetric flow rate is

$$Q = H \int u_\theta dr = \omega H \left(\frac{r_o^2 - r_i^2}{2} \right) \tag{1}$$

which is constant and independent of the induced currents since the solid disc is maintained with a constant rotation. This is

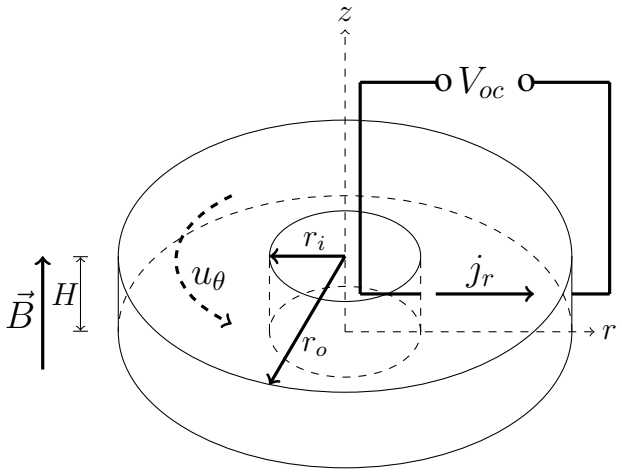

Fig. 6. Scheme of analytical problem.

commonly found in experimental setups in the laboratory.

The explored conditions for velocity ($\vec{u} = u_\theta(r)\hat{\theta}$) and magnetic field ($\vec{B} = B_0\hat{z}$) lead to induced electric currents $\vec{J}$ in the radial direction, namely, $\vec{J} = j_r(r)\hat{r}$. It follows that

$$\vec{E} = -\nabla\phi = E_r\hat{r} = \frac{d\phi}{dr}\hat{r} \tag{2}$$

where ϕ is the associated electric potential. With these assumptions, the radial component of Ohm's Law is

$$j_r = \sigma\left(-\frac{d\phi}{dr} + \omega B_0 r\right) \tag{3}$$

From the charge conservation equation $\nabla \cdot \vec{J} = 0$ we have that $j_r \sim r^{-1}$, or

$$j_r = \frac{C}{r} = \frac{\sigma C_f}{r} \tag{4}$$

where we have defined $C = \sigma C_f$ for convenience, and whose value will be determined. Comparing 3 and 4 leads to

$$\frac{\sigma C_f}{r} = \sigma\left(-\frac{d\phi}{dr} + \omega B_0 r\right) \tag{5}$$

from which the equation for the electric potential can be obtained as

$$\frac{d\phi}{dr} = \omega B_0 r - \frac{C_f}{r} \tag{6}$$

To obtain the electric potential between the terminals we establish the boundary conditions at the outer and inner electrodes as $\phi_f(r_o) = 0$ and $\phi_f(r_i) = \Phi_0$, respectively. Φ_0 corresponds to the potential drop measured between the terminals, obtained as

$$\Phi_0 = \frac{\omega B_0 r^2}{2} - C_f \ln(r) + A_F \tag{7}$$

with

$$C_f = \frac{\Phi_0 + B_0 Q/H}{\ln(r_o/r_i)} \tag{8}$$

$$A_F = \frac{2\Phi_0 \ln(r_o) + \omega B_0 (r_o^2 ln(r_i) - r_i^2 \ln(r_0))}{2\ln(r_o/r_i)} \tag{9}$$

From these expressions, E_r and j_r can be deduced straightforwardly. The total induced voltage V_T between the terminals along the specified path C is

$$V_T = -\int_C \vec{E} \cdot \vec{dl} = -\Phi_0 \tag{10}$$

The total current I_T that flows through the system is obtained from the surface integration of j_r and the equation $\frac{d\phi}{dr} = \omega B_0 r - \frac{C_F}{r}$, leading to

$$I_T = \frac{V_{oc}}{R_i}(1 - K) \tag{11}$$

where

$$V_{oc} = \frac{B_0 Q}{H} \tag{12}$$

is the open circuit voltage, and K is the load factor parameter defined as

$$K = \frac{V_T}{V_{oc}} \tag{13}$$

Alternatively, the load factor can be expressed in terms of the internal resistance R_i equal to

$$R_i = \frac{\ln(r_o/r_i)}{2\pi\sigma H} \tag{14}$$

and an external resistance R_k [10]. If a load resistance R_k is connected to the circuit the total voltage can be expressed as $V_T = R_k I_T$. The total electric power is then

$$P_e = V_T I_T = \frac{V_{oc}^2}{R_i}(1 - K)\, K \tag{15}$$

From (15), the maximum electrical power transfer is obtained when $K = 1/2$, which means that the external resistance is the same as the internal resistance of the system which is not easily attained.

IV. Results and Discussion

In this section, the analytical model are compared with experimental results. Firstly, we address the case in which the Faraday's disc operates in open circuit conditions at different rotation speeds. Then, in the second subsection, we explore the effect of an external load on the electrical variables of the system. This later analysis considers only the analytical model.

A. Models comparison in open circuit configuration

At this stage, the open circuit test applied to generator models is carried out. The test consists of performing the voltage measurement on the inner and outer radii of the conductive disc while the disc rotates at five different speeds. These speeds were restricted by the driving motor used in the experiments that ensure a smooth operation, that is to say, clogging is minimized. For this test, only one design has been used (see Table I). Therefore, the air gap between the magnet and the disc, the magnetic field strength, and the conductivity of the disc were considered constant. The values of all these variables have been used for the analytical model. Table II presents the induced voltage for all considered velocities obtained from the analytical model and experimental measurements. The induced voltage as a function of the rotation frequency is shown in Figure 7. Measured induced voltage ranges from 2.94 - to 6.55 mV. From the analytical results, a monotonous increase of the induced voltage with respect to the rotation speed is observed. For the experimental results, this is not the case. At 1855 and 2027 RPM unexpected behavior was observed. A closer look at the experiment showed relevant facts for explored rotation speeds:

- there is not good electrical contact between the electrodes and the aluminum disc due to the wobbling of the disc induced by misalignment,
- fluctuation in speed due to the forcing element (DC motor) affects the mechanical performance of the system,
- measurements are not done exactly on the inner surface of the disc due to the experimental setup,
- disc wear produced by friction with the testing probes.

Moreover, these effects are not equal for all speeds. This suggests that as the disc increases its speed, it significantly affects the contact resistance and mechanical friction for the terminal pins that collect the voltage. Although the measurements do not show a good agreement with the analytical model, the experimental results are in the same order of magnitude as those of the analytical model and are prone to be improved.

TABLE II
Experimental and Analytical Induced Voltage for Different Rotation Frequencies

Frequency	**Tangential velocity**[a]	**Induced Voltage**	
[RPM]	[m s^{-1}]	Experimental	Analytical
1297	0.33, 3.39	2.94	5.54
1645	0.43, 4.30	3.38	7.03
1855	0.48, 4.85	6.55	7.93
2027	0.53, 5.30	5.99	8.66
2319	0.60, 6.07	5.33	9.91

[a] The tangential velocity is given at the inner and outer radius.

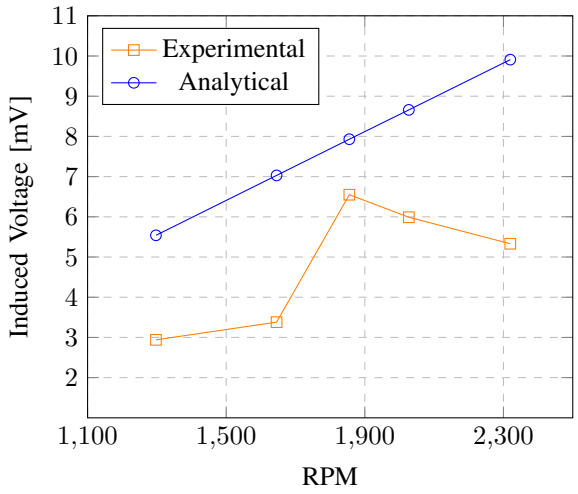

Fig. 7. Induced voltage as a function of the speed disc

B. Generator response with estimated load resistance

Developing any application using an electric generator needs to consider the connection of load resistances. The load resistance R_k is a critical value to obtain the maximum output power [12]. In order to explore the performance of the generator when an external load is connected between the terminals, we consider the analytical model but with a hypothetical load.

From (15) we observe that the maximum electrical power transfer is obtained when the external resistance equals the internal resistance. To estimate the values of the feasible R_k we could connect in the generator, it is necessary to calculate the internal resistance of the disc using the physical and geometrical parameters of the disk. For the explored case, the internal resistance is 4.84 $\mu\Omega$, which is not easily attainable in experiments. This can be verified by looking at a 10 cm-long cylindrical cable.

The diameter of this cable to build a resistance such that $R_k = R_i$, can be obtained from

$$R_k = \rho \frac{l}{a} \tag{16}$$

with ρ the resistivity, l length and a the transversal area. If the external resistance is built in aluminum, the cable's diameter would be 21.71 mm, while it would be 17.52 mm if the cable is fabricated of copper. If the resistance has a C-shape, with these dimensions, it is a problem to connect it to the inner and outer radius of the generator. Moreover, with such dimensions, the resistance should end as a pinpoint, which poses additional complications. For this case, higher attainable values of the resistance are represented in figure 8. From this figure 8 we can observe that the values in the range of mΩ correspond to a cable diameter of 0.26 and 0.19 mm, using aluminum and copper respectively. Thus, a resistance of $R_k = 4.84$ mΩ, can be easily reached in the laboratory.

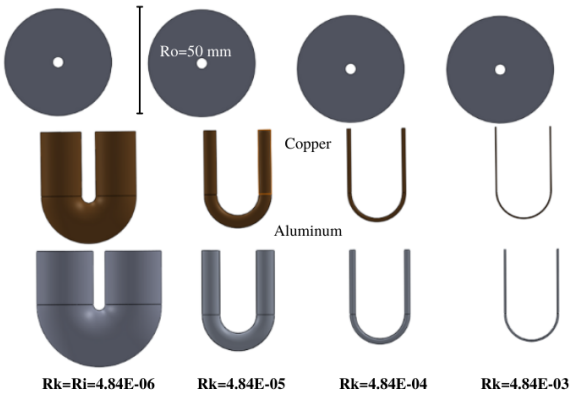

Fig. 8. Geometric representation of the four external loads to reach a given load resistance

To demonstrate the behavior of the power that might be generated. The following figure 9 shows the electric power as a function of load resistances at different frequencies of rotation.

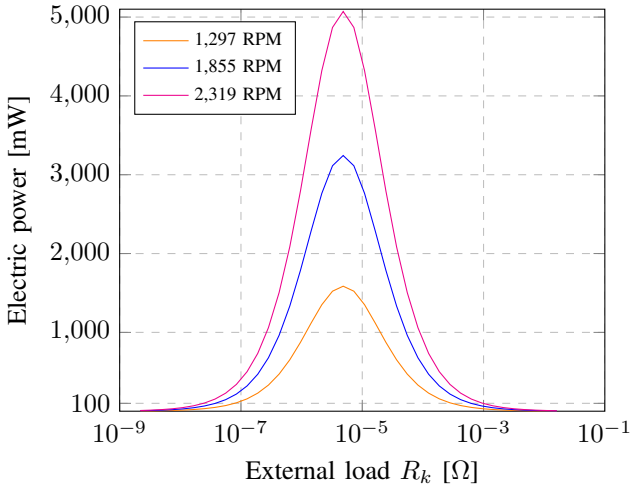

Fig. 9. Electric power as a function of the external load R_k, for 3 different frequencies of rotation

From the figure 9 we can see how the electric power grows as a function of frequency of rotation; also, we can see the behavior of the generator at different load resistance. In turn, we can notice how the maximum electric power value is found when the value of the load resistance approaches the value of the internal resistance. Another option which could be considered for experimentation is to change the dimensions of the disc according to the equation for (14), where internal disc resistance values allow a viable load resistance to be built. The following figure 10 shows the power values which could be extracted by considering two different disc sizes using aluminium and copper.

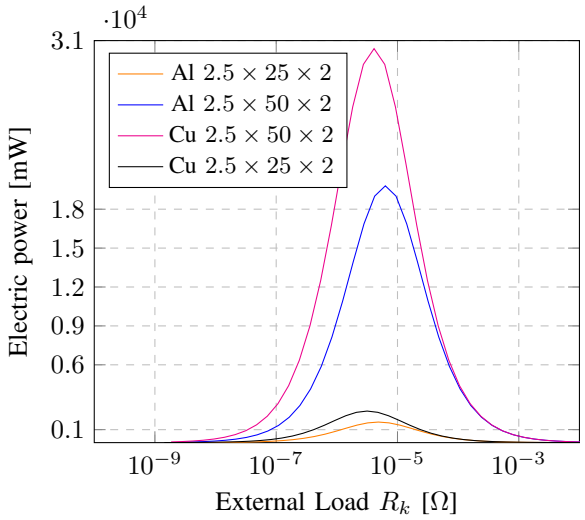

Fig. 10. Electric power as a function of the external load R_k, for aluminum $\sigma = 37.8 \times 10^6$ S m$^-$1 and copper $\sigma = 58 \times 10^6$ S m$^-$1 and 2 different disc sizes, in the graph are presented the sizes for $r_i \times r_o \times$height in mm.

It can be seen from the figure 10 for different materials and sizes that increase the radius for each disc (aluminum and copper) exponentially increases the power that can be extracted. Because of the tangential speed of the external radius is greater than the internal radius, and both speeds depend on the radio, the variation is exponential as you can see in the caudal equation (1).

V. Conclusions

An electric generator of a Faraday disk type was studied, where an analytical and an experimental model were done. The analytical model considered the solid rotating disk in the presence of a homogeneous magnetic field. On the other hand, the experimental model consisted of an aluminum solid cylindrical ring-shaped disc mounted on a dc motor shaft in order to rotate it at different speeds. In both cases, a fixed cylindrical permanent magnet, whose size is identical to the solid disc, provides a constant magnetic field.

The analytical model and experimental results showed a direct relationship between the increasing generated open circuit voltage with the increase of the solid disc speed. The development of this experiment allowed us to realize the challenges to face in characterizing this type of device. In this case, the contact between the rotating disk and the construction of load resistances was found to be the most challenging task, which led to unexpected measurements under certain conditions. Yet, the obtained results permitted us to understand the main feature of a Faraday generator and identify those aspects that need attention to improve the system and reduce uncertainties.

Results are a first approximation to knowing the behavior of this loaded generator and are the base to go one step forward in the development of generators based on liquid metals.

ACKNOWLEDGMENT

The authors thank Cesar Alberto Hernández Jacobo for his technical support in the experimental implementation. M. Rivero acknowledges UNAM-DGAPA-PAPIIT Project IA100621.

REFERENCES

[1] U. E. I. Administration, "Annual energy outlook 2020," tech. rep., Jan 29, 2020.

[2] L. B. Kong, T. Li, H. H. Hng, F. Boey, T. Zhang, and S. Li, "Waste energy harvesting," *Lecture Notes in Energy*, vol. 24, pp. 263–403, 2014.

[3] T. Kaźmierski and S. Beeby, *Energy Harvesting Systems: Principles, Modeling and Applications*. SpringerLink : Bücher, Springer New York, 2010.

[4] A. Jbaily and R. W. Yeung, "Piezoelectric devices for ocean energy: a brief survey," *Journal of Ocean Engineering and Marine Energy*, vol. 1, no. 1, pp. 101–118, 2015.

[5] F.-R. Fan, Z.-Q. Tian, and Z. L. Wang], "Flexible triboelectric generator," *Nano Energy*, vol. 1, no. 2, pp. 328 – 334, 2012.

[6] M. Mariello, F. Guido, V. Mastronardi, M. Todaro, D. Desmaële, and M. D. Vittorio], "Nanogenerators for harvesting mechanical energy conveyed by liquids," *Nano Energy*, vol. 57, pp. 141 – 156, 2019.

[7] S. Khalid, I. Raouf, A. Khan, N. Kim, and H. S. Kim, "A review of human-powered energy harvesting for smart electronics: Recent progress and challenges," *International Journal of Precision Engineering and Manufacturing-Green Technology*, 2019.

[8] M. Alhawari, B. Mohammad, H. Saleh, and M. Ismail, *Energy harvesting for self-powered wearable devices*. Springer, 2018.

[9] R. Riemer and A. Shapiro, "Biomechanical energy harvesting from human motion: theory, state of the art, design guidelines, and future directions," *Journal of NeuroEngineering and Rehabilitation*, vol. 8, p. 22, 2011.

[10] R. A. Ávalos Zúñiga and M. Rivero, "Theoretical modeling of a vortex-type liquid metal mhd generator for energy harvesting applications," *Sustainable Energy Technologies and Assessments*, vol. 52, p. 102056, 2022.

[11] C. E. Bello Morales, "Caracterización electromagnética de un dínamo de disco con contactos de metal líquido.," Master's thesis, Instituto Politécnico Nacional, Centro de Investigación en Ciencia Aplicada y Tecnología Avanzada, Unidad Querétaro, 2018.

[12] R. A. Ávalos Zúñiga and M. Rivero, "Theoretical modeling of a vortex-type liquid metal mhd generator for energy harvesting applications," *Sustainable Energy Technologies and Assessments*, vol. 52, p. 102056, 2022.